Ecotoxicology and Environmental Safety 256 (2023) 114840

Contents lists available at ScienceDirect

Ecotoxicology and Environmental Safety

journal homepage: www.elsevier.com/locate/ecoenv

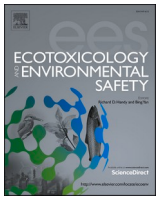

Phytosphingosine inhibits cell proliferation by damaging DNA in human cell lines

Chunxiao Sun [a,b], Xuexiu Chang [b,c], Hugh J. MacIsaac [a,c], Jiayao Wen [a], Lixing Zhao [d], Zhi Dai [d], Jiaojiao Li [a,*]

[a] School of Ecology and Environmental Science, Yunnan University, Kunming 650091, China
[b] Great Lakes Institute for Environmental Research, University of Windsor, Windsor, ON N9B 3P4, Canada
[c] College of Agronomy and Life Sciences, Kunming University, Kunming 650214, China
[d] Key Laboratory of Medicinal Chemistry for Natural Resource, Ministry of Education, Yunnan Provincial Center for Research & Development of Natural Products, School of Chemical Science and Technology, Yunnan University, Kunming 650091, China

ARTICLE INFO

Edited by Professor Bing Yan

Keywords:
Microcystis aeruginosa exudates
Cytotoxicity
CNE2 cells
Genetic toxicity
S phase

ABSTRACT

Harmful cyanobacterial blooms have caused numerous biosecurity incidents owing to the production of hazardous secondary metabolites such as microcystin. Additionally, cyanobacteria also release many other components that have not been explored. We identified compounds of a toxic mixture exudated from a dominant, blooming species, *Microcystis aeruginosa*, and found that phytosphingosine (PHS) was one of the bioactive components. Since PHS exhibited toxicity and is deemed a hazardous substance by the European Chemicals Agency, we hypothesized that PHS is a potentially toxic compound in M. *aeruginosa* exudates. However, the mechanisms of PHS ecotoxicity remain unclear. We assessed the cytotoxicity of PHS using an in vitro cell model in eight human cell lines and observed that the nasopharyngeal carcinoma cell line CNE2 was the most sensitive. We exposed CNE2 cells to 0–25 μmol/L PHS for 24 hr to explore its toxicity and mechanism. PHS exposure resulted in abnormal nuclear morphology, micronuclei, and DNA damage. Moreover, PHS significantly inhibited cell proliferation and arrested cell cycle at S phase. The results of Western blot suggested that PHS increased the expression of DNA damage-related proteins (ATM, p-P53 and P21) and decreased the expression of S phase-related proteins (CDK2, CyclinA2 and CyclinE1), indicating the toxicological mechanism of PHS on CNE2 cells. These data provide evidence that PHS has genetic toxicity and inhibits cell proliferation by damaging DNA. Our study provides evidence that PHS inhibits cell proliferation by damaging DNA. While additional work is required, we propose that PHS been considered as a potentially toxic component in MaE in addition to other well-characterized secondary compounds.

1. Introduction

Cyanobacteria are ancient, photosynthetic bacteria (Sanchez-Baracaldo et al., 2022). In recent decades, they have increasingly been associated with Harmful Algal Blooms (cHABs) in eutrophic waters (Huisman et al., 2018). Blooming cyanobacteria produce a wide range of secondary metabolites, which when released following cell lysis are harmful to animals (Codd et al., 2015), including humans (Buratti et al., 2017). Most research on these metabolites focused on toxins such as microcystins, anatoxin, and cylindrospermopsin (Sukharevich and Polyak, 2021). Cyanobacteria also continuously produce and release other poorly-studied secondary metabolites into the environment. Our former studies found that these exudates were more harmful than the aforementioned metabolites (Zheng et al., 2013). These exudates elicit cardiotoxic (Zi et al., 2018) and neurotoxic (Cai et al., 2022) effects in fish and reproductive toxicity to waterfleas (Xu et al., 2019).

Microcystis aeruginosa (Ma) is a dominant bloom-forming species of cyanobacteria (Huo et al., 2021). One compound present in the exudates of *M. aeruginosa* (MaE) is phytosphingosine (PHS) (Li et al., 2022; Zhou et al., 2023), a natural sphingolipid found in plants, fungi, and animals (Velazquez et al., 2021). The concentration of PHS in MaE ranges between 0.9 and 2.9 μg/L (Li et al., 2022). Sphingolipids are a class of cellular lipids involved in the maintenance of cell structure and mediation of cellular signaling (Hannun and Obeid, 2008). PHS is the

* Corresponding author.
E-mail address: jiaojiaoli@ynu.edu.cn (J. Li).

https://doi.org/10.1016/j.ecoenv.2023.114840
Received 28 January 2023; Received in revised form 23 March 2023; Accepted 24 March 2023

precursor of bioactive sphingolipids such as ceramides (Cer) (Chaurasia and Summers, 2015), sphingosine 1 phosphates (S1P) (Maceyka et al., 2012), Sphingosine Kinase (SphK), and sphingosine (Sph). Cer, S1P, and Sph are signaling molecules serving as intracellular second messengers, which are intimately linked to the occurrence of diseases (Hannun and Obeid, 2008; Taha et al., 2006). PHS has a similar structure to Sph but adds a hydroxyl group to the sphingoid long-chain base at C-4 (Mashima et al., 2020). PHS is listed as a corrosive and environmental hazard by European Chemicals Agency (ECHA) because it is caustic, irritating to the eyes, and very toxic to aquatic life (ECHA, 2022). Mechanistically, PHS induced apoptotic cell death in human cancer cells by activating caspase-8 and translocating Bax (Park et al., 2003a, 2003b; Li et al., 2022). PHS also caused cell death via modulating the muscarinic acetylcholine receptor (mAChR)-mediated signal transduction pathway (Lee et al., 2001). More interestingly, using a novel approach that combined machine learning and molecular docking, PHS was identified as a potential neurotoxin in MaE (Zi et al., 2022). However, the ecotoxicity of PHS, including its risk to human health, remains unclear.

Currently, the list of environmentally hazardous compounds to which humans are exposed is rapidly growing (Rasheed et al., 2019). High-throughput experimental techniques can assist in identification of toxicity of MaE compounds (Krewski et al., 2020). Cytotoxicology, a new field of in vitro toxicology, offers a more effective and efficient alternative to traditional toxicological testing based on in vivo animal tests (Rehberger et al., 2018). Human cytotoxicology is also developing rapidly, with numerous various human cell lines established (Kolman, 2003). A previous study used rat and human cell lines to assess the cytotoxicity of crude cyanobacterial extracts, and the findings provided basic data for the toxicological monitoring of cyanobacteria (Hrouzek et al., 2016). Cell viability and proliferation are typical indicators for evaluating compound toxicity and are important basic human functions (Adan et al., 2016; Zödl et al., 2004). Cell proliferation is accomplished via the process of the cell cycle (Alenzi, 2004). The process of the cell cycle is precisely controlled, including the G0/G1 phase, S phase (DNA synthesis), G2 phase, and M phase (mitosis) (Ding et al., 2020). In addition, many activities are involved in cell proliferation, such as DNA replication, related protein expression, and normal activity of cellular organelles. Previous studies found that 20 μM PHS inhibited the growth of Chinese hamster ovary cells (Lee et al., 2001), while 1 μg/ml PHS reduced cell growth in human malignant myeloid K562 cells (Han et al., 2015). However, the mechanism of anti-proliferative toxicity of PHS has not been determined.

In this study, we used the in vitro human cell model to explore the ecotoxicological effects of PHS. We evaluated cytotoxicity of PHS using eight types and investigated effects on DNA, chromosomes, nuclei, and cell cycle. We then revealed the molecular link between DNA damage and S phase arrest.

2. Materials and methods

2.1. Cell cultures and chemical preparation

Cell lines including human non-small cell lung carcinoma H1299, human ovarian carcinoma SKVO3, human hepatocellular carcinoma HepG2 and MHCC97H, human glioblastoma multiform tumors T98G, human embryonic kidney (HEK)− 293 T, human umbilical vein endothelial (HUVEC) and CNE2 cells were supplied by the School of Chemical Science and Technology of Yunnan University (Kunming, China). CNE2 cell line was certified by STR analysis. Cells were cultured in Dulbecco's modified Eagle's medium (DMEM) (Gibco, USA) supplemented with 10% (v/v) heat-inactivated fetal bovine serum (Gibco, USA) in a humidified incubator at 37 ℃ in an atmosphere of 5% CO_2. PHS (CAS: 554–62–1) was purchased from Yuanye, Shanghai, China. Freshly-prepared PHS solution was used for each experiment.

2.2. Cell viability assay

Cell viability was examined by using the 3-(4,5-dimethylthiazol-2-yl)− 5-(3-carboxy methoxyphenyl)− 2-(4-sulfophenyl)− 2 H-tetrazolium (MTS) assay. Cells were seeded into 96-well plates in 100 μl medium and 5×10^3 cells and allowed to grow and attach for 24 hr in the incubator. Stable growing cells were exposed to different PHS concentrations for 24 h. Subsequently, the medium was removed, and 100 μl MTS (10%) with DMEM (90%) mixed solution was added for 30–40 min exposure in a dark incubator at 37 ℃. The absorbance of formazan for each well was measured at 490 nm using a microplate reader (Epoch, Bio-Tek). We calculated relative cell viability as follows: (Absorbance of the treated wells / Absorbance of the untreated wells) × 100%. The calculation of the half maximal inhibitory concentration (IC_{50}) fit curve was performed by GraphPad 9.0 software.

2.3. Detection of cell proliferation

Cell proliferation was reflected by cell number changes over time and the distribution of the cell cycle. CNE2 was seeded into 6-well plates with 1×10^5 cells/well. After 24 hr growth, cells were exposed to different concentrations of PHS, and living cells were counted every 12 h using a hemocytometer.

The cell cycle distribution was measured by a cell-cycle detecting kit (Solarbio, China). CNE2 cells were treated with different concentrations of PHS for 24 h. 1×10^6 cells were collected per treatment, washed by PBS, and fixed in 70% ethanol overnight at 4 ℃. The cells were rewashed with PBS to remove the fixative, then 100 μl RNase solution was added, heated at 37 ℃ for 30 min, and stained with PI for 20 min in the dark. The DNA content was detected using flow cytometry and analyzed using ModFit LT 5.0 software.

2.4. Detecting the effects of PHS on nuclei and chromosomes

To investigate the effect of PHS on the CNE2 nucleus - the important organelle in S phase - we evaluated the damage to nuclei and chromosomes.

We visualized nuclear morphology using Hoechst 33342 fluorescence staining. CNE2 cells (2×10^4 cells/well) were seeded into 24-well plates and treated with different concentrations of PHS for 24 hr. Cells were then stained by Hoechst 33342 (Solarbio, China) solution (10 μg/ml) for 20 min in the dark at room temperature. To remove the staining solution, we washed cells by PBS with shaking. Stained blue nuclei were detected by fluorescence microscopy. Normal nuclear chromatin was evenly distributed, while that of abnormal chromatin was aggregated and fragmented. The rate of the abnormal nucleus was calculated as abnormal nucleus cell number / total cell number. A minimum of 1000 cells were counted per sample.

We used the cytokinesis-blocking micronucleus (CBMN) assay to assess chromosomes (Fenech, 2007). CNE2 cells were seeded into 6-well plates and treated with PHS for 24 hr. PHS was withdrawn after the treatment time, and cytochalasin B was added to the culture for the next 24 hr. Prepared cell slides were stained with Wright-Giemsa solution (Solarbio, China) and analyzed under the microscope. The rate of micronuclei (MNi) was calculated as MNi cell number / total cell number. A minimum of 100 cells were counted per sample.

2.5. Detection of DNA damage

Single-cell gel electrophoresis (SCGE), commonly known as the comet assay, is a sensitive method for detecting DNA breaks in single cells (Singh et al., 1988). We first prepared a layer of 0.5% normal melting agarose (NMA) to place on the slide as the initial layer of gel. We then collected CNE2 cells after being exposed to different PHS concentrations for 24 hr and resuspended in PBS. As the second layer of gel, 10 μl of cell suspension (1×10^6 cells/ml) and 75 μl of 0.7% low melting

agarose (LMA), mixed at 37 ℃, were put on comet slides and covered with coverslip at 4 ℃ for 30 min. The comet slides were then placed in lysing buffer at 4 ℃ for 2 hr in the dark. Slides were removed from the lysing buffer, immersed in alkaline solution at room temperature for 30 min in the dark, and electrophoresed at low voltage (25 V, 300 mA) for 30 min. After being removed from the electrophoresis tank, we washed slides thrice by PBS at room temperature. Slightly air-dried slides were stained for 20 min in the dark with propidium iodide (PI), photographed using fluorescence microscopy, and analyzed using CASP software, with 50 cells analyzed per sample. DNA in the head (%), DNA in the tail (%), and the olive tail moment (OTM) were applied to evaluate DNA damage. OTM is DNA in the tail (%) × the distance from the head's center to the tail's center. The degree of DNA damage was assessed (Anderson et al., 1994).

We measured DNA synthesis using an EdU (5 – Ethynyl - 2′ - deoxyuridine) Apollo567 in vitro kit (Solarbio, China). CNE2 cells (2×10^4 cells/well) were seeded in 24-well plates and treated with PHS for 24 hr. Cells were grown for 4 hr in DMEM medium with EdU (50 μM), then fixed in 4% paraformaldehyde (PFA) for 30 min at room temperature and permeabilizated with 0.5% TritonX-100 for 10 min. Apollo 567 (1X) was used to stain the cell for 30 min, and Hoechst 33342 was used to locate nuclei. Random fields were observed by fluorescence microscopy and the proportion of EdU-positive cells (%) was counted as the EdU-positive cell number / the total cell number.

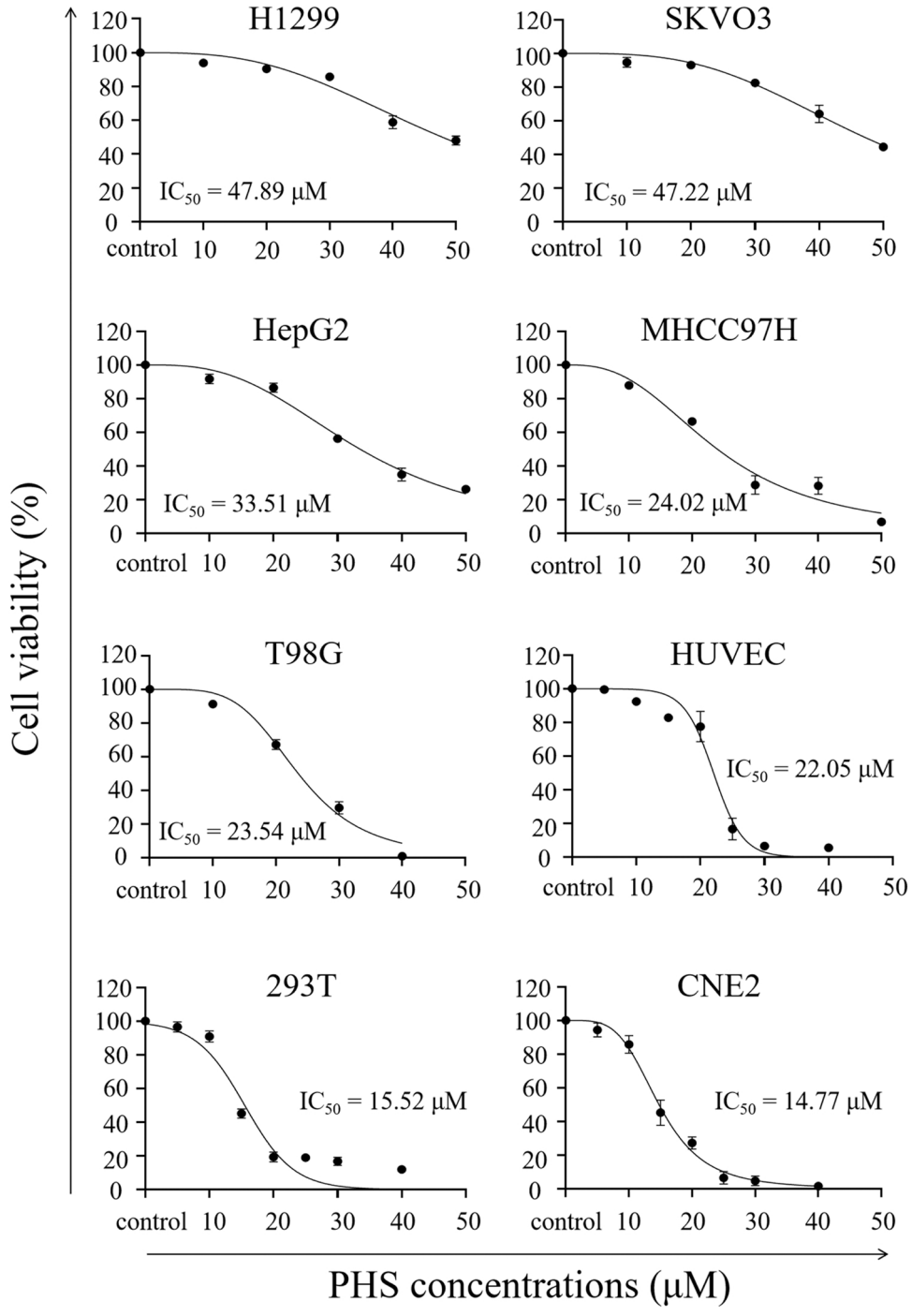

Fig. 1. Cell viability of eight types of human cell lines treated with different PHS concentrations for 24 h. Values are expressed as the mean ± SD. N = 3.

2.6. Ultrastructure of cells

CNE2 cells were seeded into 6-well plates and incubated for 24 h, following which cells were treated with PHS for 24 h. Cells were then fixed with 2.5% glutaraldehyde. The cells then underwent postfixation with 1% OsO_4 in 0.1 M cacodylate buffer followed by dehydration, cutting, and staining. Photographs were taken by transmission electron microscope (TEM) (Servicebio, China).

2.7. Western blot

We seeded CNE2 cells into 10 cm culture dishes and incubated for 24 h. After being treated with PHS for 24 h, we harvested and lysed cells. We measured total protein of CNE2 cells by the bicinchoninic acid (BCA) protein assay. Equal amounts of lysate protein (30 μg) were loaded on 10% SDS-polyacrylamide gels and electrophoretically transferred to polyvinylidene fluoride (PVDF) membranes. After blocking, the membranes were incubated overnight at 4 ℃ with primary antibodies (ATM, p-ATM, p-P53, P21, CDK2, CyclinA2, CyclinE1, GAPDH, and β-actin) (CST, Danvers, MA, USA). We incubated protein bands with corresponding secondary antibodies and then detected proteins with enhanced chemiluminescence detection reagents.

2.8. Statistical analysis

All experiments were repeated three times. Differential significance analysis and correlation analysis were performed by Origin 2018 software. Data were expressed as mean ± Standard Deviation (SD). One-way analysis of variance (ANOVA) was used to test for differences among all treatments.

3. Results

3.1. The cytotoxicity of PHS

PHS decreased the cell viability of H1299, SKVO3, HepG2, MHCC97H, T98G, HUVEC, 293 T, and CNE2 cell lines in a direct dose-dependent manner (Fig. 1). PHS also had cytotoxicity effects on these human cell lines. The H1299 cell line had the highest PHS IC_{50} value at 47.89 μM, while the CNE2 cell line had the lowest at 14.77 μM (Fig. 1). The CNE2 cell line was more sensitive to PHS than other cell lines and could be used to assess mechanisms of PHS cytotoxicity.

3.2. PHS inhibits CNE2 cell proliferation

Cell proliferation was inversely related to dose, with treated with cell numbers of 1.58, 1.39, 0.72, and 0.34 × 10^6 cells at PHS doses of 2, 4, 6, and 8 μM, while it was 1.61 × 10^6 cells in the control (Fig. 2a). PHS inhibited cell proliferation when the concentration of PHS increased from 2 μM to 8 μM. Moreover, this anti-proliferation effect was strengthened as the time interval was extended from 12 to 72 hr. Compared with the control treatment, which increased the number of cells by about 1.42 × 10^6 cells, the 8 μM PHS treatment group increased by only 1.5 × 10^5 cells (Fig. 2a). Hence, PHS inhibited the proliferation of CNE2 cells in a dose- and time-dependent.

We found that compared with the control treatment, the PHS treatments of 10, 15, 20, and 25 μM experienced significant reductions in the percentage of CNE2 cells in G0/G1 phase, while those in S phase increased significantly ($p < 0.05$, Fig. 2b). For example, treatment of 15 μM PHS resulted in the highest percentage of S phase cells (63%) ($p < 0.0001$, Fig. 2b), and the lowest percentage of G0/G1 phase (29%) ($p < 0.0001$, Fig. 2b). PHS-treated CNE2 cells arrested in S phase, thereby increasing their percentage representation, whereas representation by G0/G1 phase cells declined. The picture of cell cycle distribution visually demonstrated that PHS induced debris and aggregate cells, while the S phase increased as well (**Appendix** Fig. S1). Therefore,

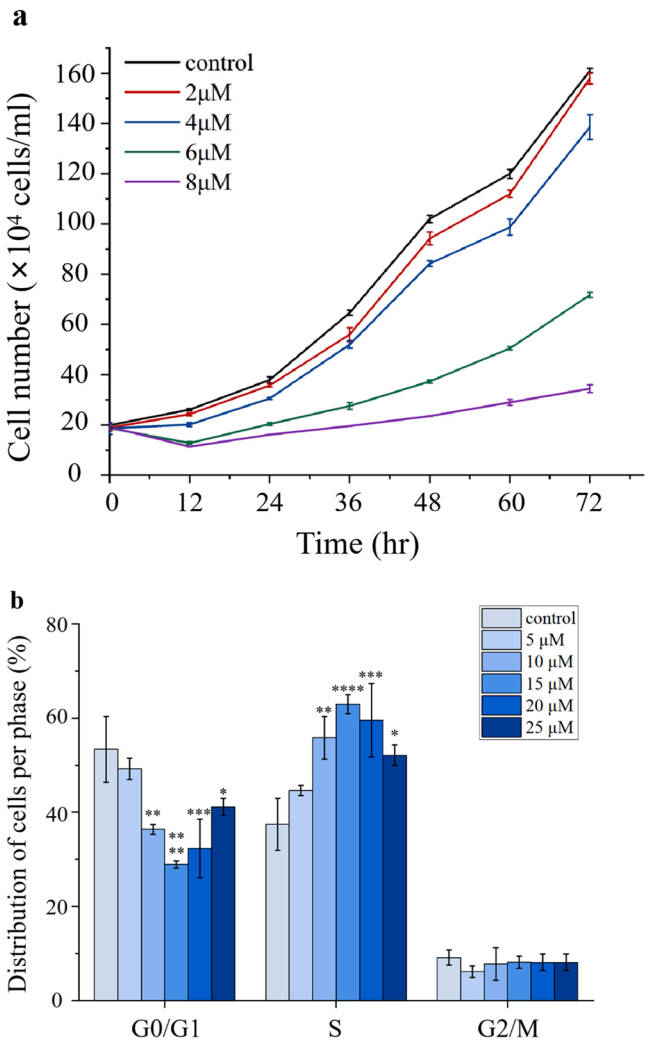

Fig. 2. (a) Cell proliferation of CNE2 cells treated with different PHS concentrations at different time points. (b) The cell cycle distribution of CNE2 cells treated with different PHS concentrations for 24 hr. Values are expressed as the mean ± SD. N = 3. * $p < 0.05$, * * $p < 0.01$, * ** $p < 0.001$, * ** * $p < 0.0001$ vs. control.

PHS induced cell cycle arrest in S phase, preventing CNE2 cells from proliferating.

3.3. PHS induces the abnormal nuclei and MNi of CNE2 cells

The graphs of nuclear morphology demonstrated that CNE2 cells had characteristics typical of abnormal nuclei, including chromatin condensation and nucleus fragmentation (**Appendix** Fig. S2a). Furthermore, when compared to the control treatment, the rate of abnormal nuclei of CNE2 cells treated with PHS increased significantly in a dose-dependent manner ($p < 0.01$, Fig. 3a). Among them, the percentage of abnormal nuclei treated with 25 μM PHS was the highest (60%), compared to the control treatment, it increased by 52% ($p < 0.0001$, Fig. 3a).

Compared to the control group (3%), the rate of MNi increased significantly in a dose-dependent manner ($p < 0.01$, Fig. 3**b,**). For example, after treatment with 5, 10, 15, 20, and 25 μM PHS for 24 hr, the rate of MNi was 5%, 8%, 10%, 13%, and 14%, respectively. Furthermore, PHS-induced nuclear buds (NBUDs) and apoptosomes in CNE2 cells (**Appendix** Fig. S2b). The CBMN assay indicated that PHS caused chromosomal abnormalities in CNE2 cells.

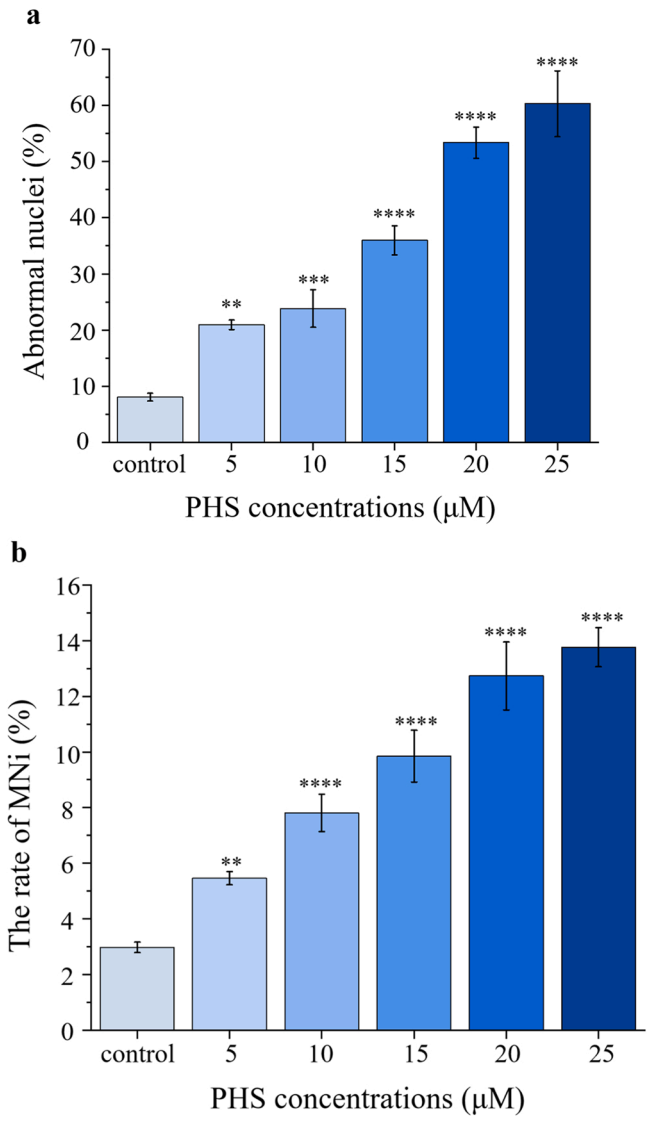

Fig. 3. (a) The rate of the abnormal nuclei of CNE2 cells treated with different PHS concentrations for 24 hr. (b) The rate of MNi of CNE2 cells treated with different PHS concentrations for 24 hr. Values are expressed as the mean ± SD. N = 3. * $p < 0.05$, * * $p < 0.01$, * ** $p < 0.001$, * ** * $p < 0.0001$ vs. control.

3.4. PHS induces DNA damage of CNE2 cells

DNA fragmentation produced the 'comet tail' phenomenon. After PHS treatment for 24 hr, the heads of the CNE2 nuclei were diminished, while the tails were lengthened (**Appendix** Fig. S3). By analyzing the content of DNA, we observed that the DNA in the comet head (%) decreased significantly ($p < 0.0001$, Fig. 4**a**) while that in the comet tail increased significantly ($p < 0.0001$, Fig. 4**b**). DNA in the tail was highest (42%) ($p < 0.0001$, Fig. 4**a**) in the 20 μM PHS treatment, while DNA in the head was lowest (58%) ($p < 0.0001$, Fig. 4**b**). The OTM value also increased significantly in a dose-dependent manner ($p < 0.01$, Fig. 4**c**), with the value highest (29%) in the 25 μM PHS treatment ($p < 0.0001$, Fig. 4**c**). These indicators suggest that PHS caused DNA fragmentation in CNE2 cells. DNA damage level was evaluated as grade II with 5, 10, and 25 μM PHS treatments, while it increased to grade III in 15 and 20 μM PHS treatments (Table 1). Compared to the control treatment, the EdU-positive cells in the PHS-treated treatment decreased significantly in a dose-dependent manner ($p < 0.05$, Fig. 4**d**). PHS inhibited DNA synthesis in CNE2 cells, which is also a type of DNA damage caused by PHS.

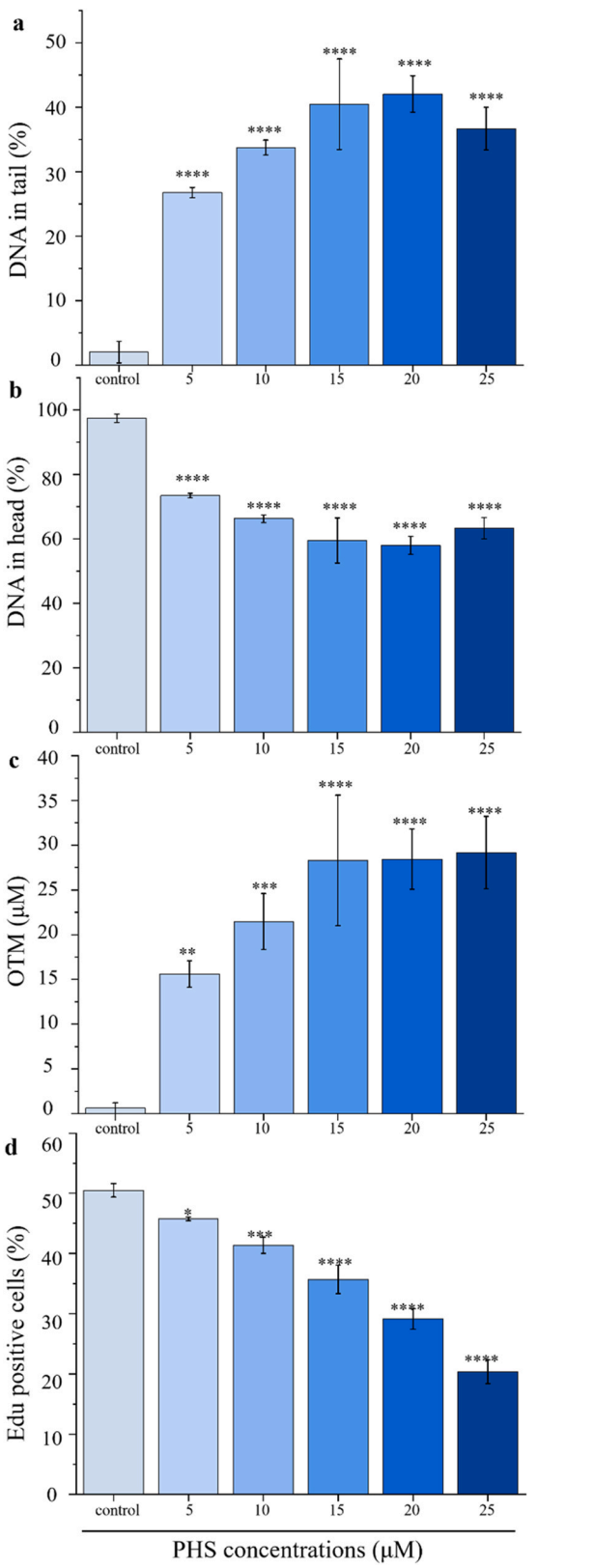

Fig. 4. Index of (a) DNA in tail; (b) DNA in head and (c) OTM in CNE2 cells, exposed to different PHS concentrations for 24 hr. (d) The rate of DNA synthesis of CNE2 cells treated with different PHS concentrations for 24 hr. Values are expressed as the mean ± SD. N-3. * $p < 0.05$, * * $p < 0.01$, * ** $p < 0.001$, * ** * $p < 0.0001$ vs. control.

Table 1
DNA damage grades (Anderson et al., 1994).

PHS concentrations (μM)	DNA in tail (%)	DNA damage grade
Control	2.0	0
5	26.8	II
10	33.7	II
15	40.5	III
20	42.1	III
25	36.7	II

3.5. PHS modulates expression of DNA damage and cell cycle-related proteins

We observed that expression of p-ATM (13 and 21 -fold), p-P53 (1.5 and 1.7 -fold), and P21 (3.1 and 3.4 -fold) increased significantly ($p < 0.05$, Fig. 5a and c) when treatment with 15 and 20 μM PHS, respectively. PHS activated expression of DNA damage-related proteins. Conversely, expression of CDK2 and CyclinE1 decreased significantly ($p < 0.05$, Fig. 5c) after treatment with 15 and 20 μM PHS, respectively. CyclinA2 expression was not affected after PHS treatment ($p > 0.05$, Fig. 5c).

3.6. PHS damage ultrastructure of CNE2 cells

Normal cells (control treatment) exhibited normal ultrastructural morphology of cytoplasm, cell organelles, and nuclei (Fig. 6a). With exposed to a low concentration of PHS (5 μM), cells incurred various damage including the irregular-shaped nucleus, chromatin pyknosis, umbilication, and unclear nuclear envelope (red arrow), swollen, fragmented, and vacuolized mitochondria (red oval), and autophagolysosomes (red rectangular) appeared (Fig. 6b). At a moderate concentration of PHS (15 μM), PHS induced autophagolysosomes, abnormal nuclei and MNi (yellow rectangular) in CNE2 cells (Fig. 6c). Finally, under high concentrations of PHS (25 μM), the nucleus of CNE2 cells dissolved, the nuclear membrane was broken, most organelles swelled, autophagolysosomes increased (Fig. 6d).

4. Discussion

We found that PHS had cytotoxicity in eight types of human cell lines

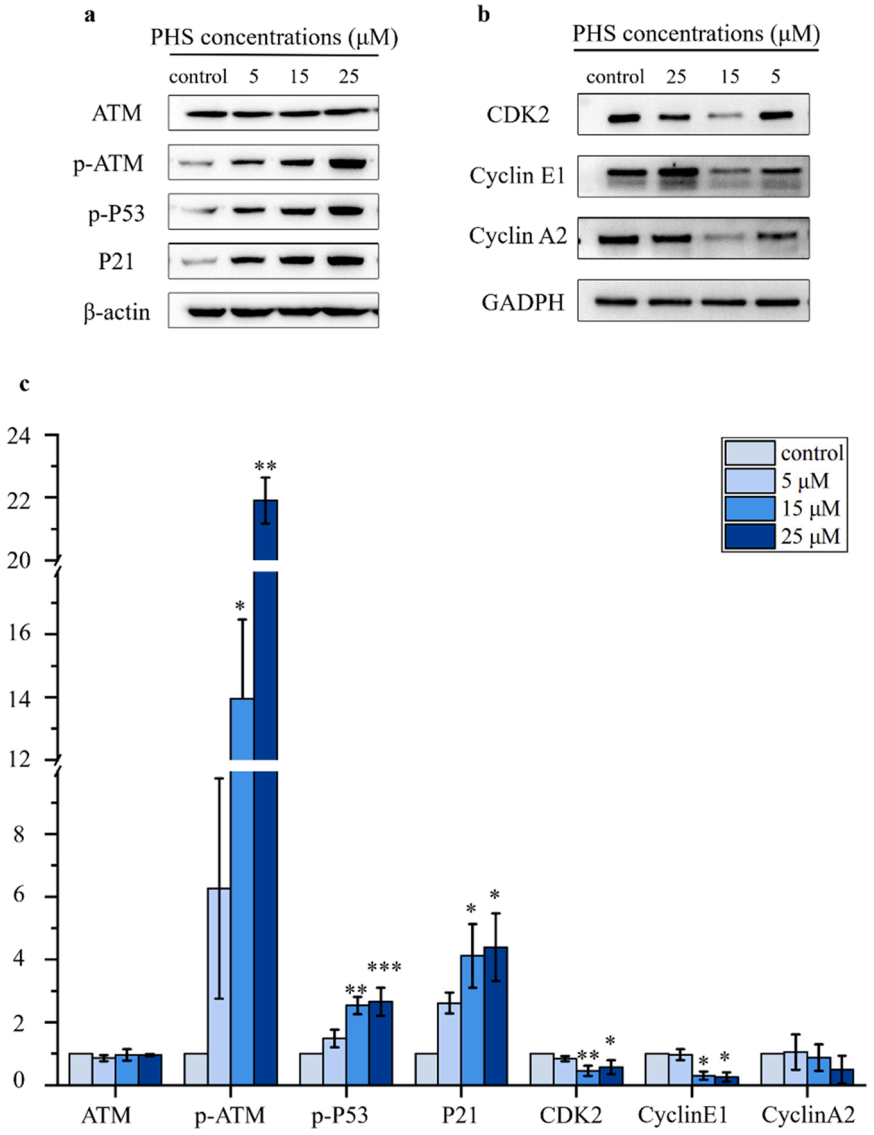

Fig. 5. (a) Western blot showed the expression of ATM, p-ATM, p-P53, P21, and β-actin in different PHS concentrations treated CNE2 cells. (c) Western blot showed the expression of CDK2, CyclinA2, CyclinE1, and GAPDH in different PHS concentrations treated CNE2 cells. (b) and (d) Quantified graphical data for protein change expression over control cell normalized to β-actin and GAPDH. Values are expressed as the mean ± SD. N = 3. * $p < 0.05$, * * $p < 0.01$, * ** $p < 0.001$ vs. control.

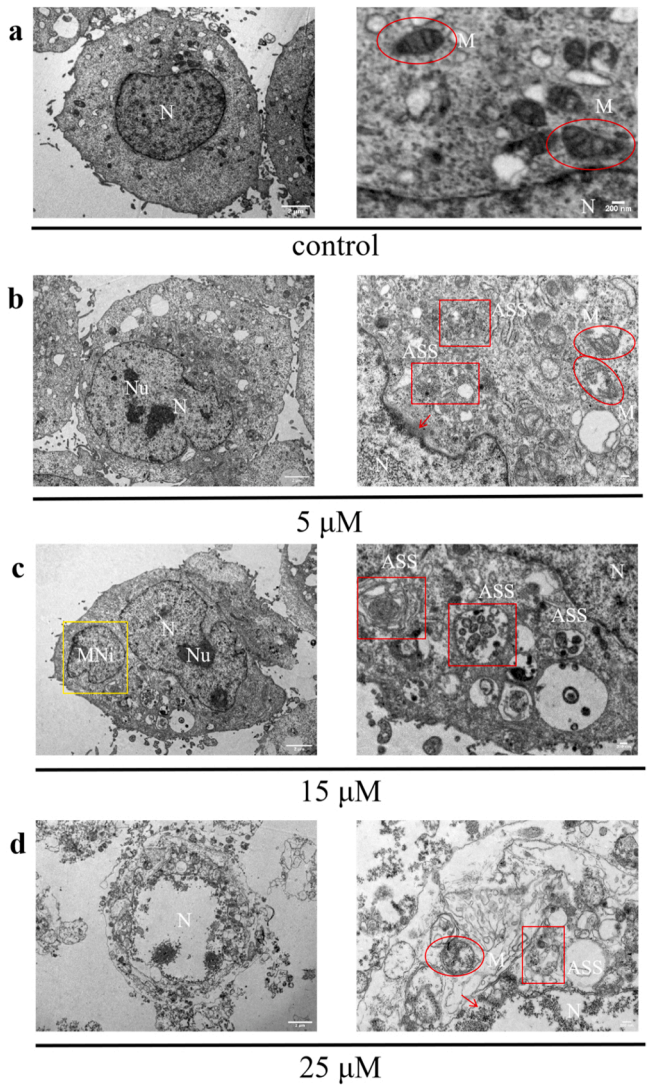

Fig. 6. TEM images of CNE2 cells (a) untreated control, exposure to (b) 5 μM, (c) 15 μM, and (d) 20 μM PHS. Abbreviations: nucleus (N), mitochondria (M) (red oval), micronuclei (MNi) (yellow rectangle), and autophagolysosomes (ASS) (red rectangle).

(Fig. 1). Our results parallel those that demonstrated PHS cytotoxicity to human T-cell lymphoma Jurkat cells (Nagahara et al., 2005), non-small cell lung cancer NCI-H460 cells (Park et al., 2003a), and human oral cells (Poulsen et al., 2015). Thus, PHS has broad-spectrum cytotoxicity to human cells. *In vitro* cytotoxicity assay results provide preliminary predictions of the harmful environmental effects of chemicals (Hrouzek et al., 2016). As a Ma exudate, PHS is potentially harmful to both aquatic and terrestrial life exposed to it. We found that CNE2 cells had the lowest IC_{50} value (Fig. 1), and thus was more sensitive to PHS than other cell lines. CNE2 cell lines are often used for toxicity testing because of its sensitivity, operability, and proliferation (Liang et al., 2019; Wang et al., 2019).

Genetic toxicity tests are a common method for assessing the toxicity of environmental contaminants (Umbuzeiro et al., 2017). We observed that PHS caused abnormalities in nuclear morphology (Fig. 3**a and Appendix** Fig. S2a) and structure (Fig. 6). Abnormal morphology of the nucleus is caused by nuclear membrane changes or abnormal division of genetic substances in the nucleus (Bian and Liu, 2014). We found that PHS primarily caused chromosomal aberration, including NBUD, MNi (Fig. 3**b**), and apoptosis cells (**Appendix** Fig. S2b). NBUDs are formed because of aberrant DNA amplification and repair, which occur frequently in the S phase (Fenech, 2007). MNi is formed when chromosomes break or vanish (Fenech, 2007). These indicators confirmed that PHS induced chromosomal damage.

DNA damage may be the main cause of nuclei and chromosome abnormalities (Janssen et al., 2011). We found that PHS induced DNA damage (Fig. 4 **and Appendix** Fig. S3) and inhibited DNA synthesis (Fig. 4**d**). Previous studies revealed that PHS induced DNA fragments in human cancer cells (Nagahara et al., 2005; Park et al., 2003b), consistent with our findings. Additionally, a number of sphingolipids similar to PHS are involved in the DNA damage response (Carroll et al., 2015). Studies on the genotoxicity of cyanotoxins have focused on DNA damage and MNi (Palus et al., 2007). Our study corroborates that PHS damages the nucleus, chromosome, and DNA, and has genetic toxicity.

We speculate that PHS induces DNA damage through the accumulation of intracellular ROS. We observed that PHS induced mitochondria damage (Fig. 6) and increased intracellular ROS levels (**Appendix** Fig. S4) in CNE2 cells. Excessive intracellular ROS can lead to DNA damage (Srinivas et al., 2019). Genotoxicity of MC is caused by its stimulation of ROS production (Svircev et al., 2010). PHS induced mitochondrial damage and DNA fragmentation in human T-cell lymphoma Jurkat cells (Nagahara et al., 2005). We observed a relationship between the accumulation of ROS and DNA damage, and speculate that PHS damaged DNA by increasing intracellular ROS levels.

We observed that PHS inhibited CNE2 cell proliferation in a time- and dose-dependent manner (Fig. 2**a**). Previous work also highlighted that PHS inhibits cell proliferation (Lee et al., 2001; Han et al., 2015). Cell proliferation inhibition is associated with abnormal progression of the cell cycle (Alenzi, 2004). Our result suggested that PHS arrested the cell cycle in S phase (Fig. 2**b**). The transition between the different phases (G1, S, G2, and M) of the cell cycle is specifically regulated by different CDKs and their activating cyclin subunits (Ding et al., 2020; Hochegger et al., 2008). The CDK2-CyclinA2 complex particularly acts during the priming and progression of DNA synthesis, and the CDK2-CyclinE1 complex promotes the G1/S transition. These complexes, consisting of CDK2, CyclnA2 and Cyclin E1, are necessary for cell cycle progression in S phase (Ding et al., 2020; Guo and Wang, 2017). The *Ganoderma lucidum* extract can arrest GBM8901 and U87 cells in the S phase by inhibiting the expression of CDK2 and cyclinA2 (Cheng et al., 2020). In our study, we found that PHS inhibited the protein expression of CDK2 and cyclinE1 (Fig. 5**c**), which induced the cell cycle arrest in S phase on CNE2 cells.

We suspect that PHS arrests the cell cycle in S phase via damaging DNA (Wang et al., 2020). We found that PHS activates proteins related to DNA damage, such as p-ATM, P53, and P21 (Fig. 5**c**). DNA damage activates ATM through phosphorylation (Bakkenist and Kastan, 2003), and the activated ATM transmits the signal to downstream proteins. Among the numerous downstream effector proteins of ATM, p53 is an important tumor suppressor protein and regulates cell cycle arrest (Chen, 2016). Activated ATM (p-ATM) can rapidly phosphorylate the ser15 site of the p53 protein (Rashid et al., 2011), and the activated p53 (p-P53) acts as a transcription factor resulting in the expression of p21 (Yagi et al., 2003), a negative regulator of the cell cycle and a family of cyclin-dependent kinase inhibitors (CDKIs). P21 arrests the cell cycle by inhibiting the CDKs activity and the complexes of CDK-Cyclin formation (Al Bitar and Gali-Muhtasib, 2019; Yagi et al., 2003). Based on our cell cycle results (Figs. 2**b and** 5**c**), it appears that PHS activates the ATM/P53/P21 pathway by damaging DNA, decreasing the expression of G2/M phase-related proteins CDK2 and CyclinE1, arresting the cell cycle in S phase and inhibiting cell proliferation. Tetra-acetyl phytosphingosine (TAPS), a phytosphingosine derivative, arrested the cell cycle in S and G2 phases on the differentiated human keratinocyte HaCaT cells, which is associated with the activity of P53 and P21 as well (Kim et al., 2003). Cer-mediated apoptosis and cell cycle arrest are due to the ability of ceramide to trigger the DNA damage response (Ahn and Schroeder, 2002; Birbes et al., 2002; Carroll et al., 2015). We observed that PHS arrested the cell cycle by damaging DNA, though we cannot exclude the

occurrence of apoptosis.

In conclusion, our study corroborates that PHS is cytotoxic and has harmful effects to human cancer cell lines. PHS inhibited the proliferation of CNE2 cells by damaging DNA, which in turn activated the ATM/P53/p21 pathway and caused the cell cycle to be arrested in S phase. Damage to DNA and chromosome highlight potential genetic toxicity of PHS, which indicated the environmental health and safety issue. We speculate that PHS causes DNA damage by accumulating intracellular ROS. While the toxicity of pure PHS was demonstrated by this study, but it is important to explore whether similar problems occur in nature during cyanobacterial blooms.

CRediT authorship contribution statement

Chunxiao Sun: Writing – original draft, Writing – review & editing, Visualization, Data curation. **Xuexie Chang:** Conceptualization, Supervision, Funding acquisition, Supervision. **Hugh J. MacIsaac:** Conceptualization, Data curation, Writing – original draft, Writing – review & editing. **Jiayao Wen:** Formal analysis, Data curation. **Lixing Zhao:** Validation, Resources. **Zhi Dai:** Formal analysis. **Jiaojiao Li:** Validation, Formal analysis, Resources, Methodology, Data curation, Funding acquisition, Project administration.

Declaration of Competing Interest

The authors declare that they have no known competing financial interests or personal relationships that could have appeared to influence the work reported in this paper.

Data Availability

Data will be made available on request.

Acknowledgments

This research was financially supported by the National Natural Science Foundation of China (No. 32101361), National Natural Science Foundation of China (NSFC) - Yunnan Joint Key Grant (No. U1902202), Yunnan Provincial Science and Technology Department grants (Nos. 202201AT070177, 2018DG005, 202101AU070078, 2019FA043), China Scholarship Council (CSC) fund, and NSERC Canada.

Appendix A. Supporting information

Supplementary data associated with this article can be found in the online version at doi:10.1016/j.ecoenv.2023.114840.

References

Adan, A., Kiraz, Y., Baran, Y., 2016. Cell proliferation and cytotoxicity assays. Curr. Pharm. Biotechnol. 17 (14), 1213–1221. https://doi.org/10.2174/1389201017666160808160513.

Ahn, E.H., Schroeder, J.J., 2002. Sphingoid bases and ceramide induce apoptosis in HT-29 and HCT-116 human colon cancer cells. Exp. Biol. Med. 227 (5), 345–353. https://doi.org/10.1177/153537020222700507.

Al Bitar, S., Gali-Muhtasib, H., 2019. The role of the cyclin dependent kinase inhibitor p21(cip1/waf1) in targeting cancer: Molecular mechanisms and novel therapeutics. Cancers 11 (10), 1475. https://doi.org/10.3390/cancers11101475.

Alenzi, F.Q., 2004. Links between apoptosis, proliferation and the cell cycle. Br. J. Biomed. Sci. 61 (2), 99–102. https://doi.org/10.1080/09674845.2004.11732652.

Anderson, D., Yu, T.W., Phillips, B.J., Schmezer, P., 1994. The effect of various antioxidants and other modifying agents on oxygen-radical-generated DNA damage in human lymphocytes in the COMET assay. Mutat. Res. 307 (1), 261–271. https://doi.org/10.1016/0027-5107(94)90300-x.

Bakkenist, C.J., Kastan, M.B., 2003. DNA damage activates ATM through intermolecular autophosphorylation and dimer dissociation. Nature 421 (6922), 499–506. https://doi.org/10.1038/nature01368.

Bian, G., Liu, R., 2014. Field investigation on genotoxicities of Zhangze reservoir water body to *Rana nigromaculata* tadpoles. Asian J. Ecotoxicol. 9 (6), 1126–1132. https://doi.org/10.7524/AJE.1673-5897.20140709002.

Birbes, H., El Bawab, S., Obeid, L.M., Hannun, Y.A., 2002. Mitochondria and ceramide: intertwined roles in regulation of apoptosis. Adv. Enzym. Regul. 42, 113–129. https://doi.org/10.1016/s0065-2571(01)00026-7.

Buratti, F.M., Manganelli, M., Vichi, S., Stefanelli, M., Scardala, S., Testai, E., et al., 2017. Cyanotoxins: producing organisms, occurrence, toxicity, mechanism of action and human health toxicological risk evaluation. Arch. Toxicol. 91 (3), 1049–1130. https://doi.org/10.1007/s00204-016-1913-6.

Cai, W., MacIsaac, H.J., Xu, R., Zhang, J., Pan, X., Zhang, Y., et al., 2022. Abnormal neurobehavior in fish early life stages after exposure to cyanobacterial exudates. Ecotoxicol. Environ. Saf. 245, 114–119. https://doi.org/10.1016/j.ecoenv.2022.114119.

Carroll, B., Donaldson, J.C., Obeid, L., 2015. Sphingolipids in the DNA damage response. Adv. Biol. Regul. 58, 38–52. https://doi.org/10.1016/j.jbior.2014.11.001.

Chaurasia, B., Summers, S.A., 2015. Ceramides - lipotoxic inducers of metabolic disorders. Trends Endocrinol. Metab. 26 (10), 538–550. https://doi.org/10.1016/j.tem.2015.07.006.

Chen, J., 2016. The cell-cycle arrest and apoptotic functions of p53 in tumor initiation and progression. Cold Spring Harb. Perspect. Med 6 (3), a026104. https://doi.org/10.1101/cshperspect.a026104.

Cheng, A.Y., Chien, Y.C., Lee, H.C., Hsieh, Y.H., Yu, Y.L., 2020. Water-extracted *Ganoderma lucidum* induces apoptosis and S-phase arrest via Cyclin-CDK2 pathway in glioblastoma cells. Molecules 25 (16), 3585. https://doi.org/10.3390/molecules25163585.

Codd, G.A., Pliński, M., Surosz, W., Hutson, J., Fallowfield, H.J., 2015. Publication in 1672 of animal deaths at the Tuchomskie Lake, northern Poland and a likely role of cyanobacterial blooms. Toxicon 108, 285–286. https://doi.org/10.1016/j.toxicon.2015.10.005.

Ding, L., Cao, J., Lin, W., Chen, H., Xiong, X., Ao, H., et al., 2020. The roles of cyclin-dependent kinases in cell-cycle progression and therapeutic strategies in human breast cancer. Int. J. Mol. Sci. 21 (6), 1960. https://doi.org/10.3390/ijms21061960.

European Chemicals Agency (ECHA), 2022. Substance information for NO. 439–210-6, (2S, 3S, 4R)- 2 - aminooctadecane- 1, 3, 4- triol. Available: ⟨https://echa.europa.eu/substance-information/-/substanceinfo/100.103.588⟩. Accessed September 30, 2022.

Fenech, M., 2007. Cytokinesis-block micronucleus cytome assay. Nat. Protoc. 2 (5), 1084–1104. https://doi.org/10.1038/nprot.2007.77.

Guo, H., Wang, M., 2017. Dichloromethane fraction of *Asiasarum heterotropoides* induces S phase arrest and apoptosis in KB oral epithelial carcinoma cells. Biomed. Pharmacother. 89, 559–564. https://doi.org/10.1016/j.biopha.2017.02.072.

Han, S.H., Kim, J., Her, Y., Seong, I., Park, S., Bhattarai, D., Jin, G., et al., 2015. Phytosphingosine promotes megakaryocytic differentiation of myeloid leukemia cells. BMB Rep. 48 (12), 691–695. https://doi.org/10.5483/bmbrep.2015.48.12.100.

Hannun, Y.A., Obeid, L.M., 2008. Principles of bioactive lipid signalling: lessons from sphingolipids. Nat. Rev. Mol. Cell Biol. 9 (2), 139–150. https://doi.org/10.1038/nrm2329.

Hochegger, H., Takeda, S., Hunt, T., 2008. Cyclin-dependent kinases and cell-cycle transitions: does one fit all? Nat. Rev. Mol. Cell Biol. 9 (11), 910–916. https://doi.org/10.1038/nrm2510.

Hrouzek, P., Kapuścik, A., Vacek, J., Voráčová, K., Paichlová, J., Kosina, P., et al., 2016. Cytotoxicity evaluation of large cyanobacterial strain set using selected human and murine in vitro cell models. Ecotoxicol. Environ. Saf. 124, 177–185. https://doi.org/10.1016/j.ecoenv.2015.10.020.

Huisman, J., Codd, G.A., Paerl, H.W., Ibelings, B.W., Verspagen, J.M.H., Visser, P.M., 2018. Cyanobacterial blooms. Nat. Rev. Microbiol. 16 (8), 471–483. https://doi.org/10.1038/s41579-018-0040-1.

Huo, D., Gan, N., Geng, R., Cao, Q., Song, L., Yu, G., et al., 2021. Cyanobacterial blooms in China: diversity, distribution, and cyanotoxins. Harmful Algae 109, 102106. https://doi.org/10.1016/j.hal.2021.102106.

Janssen, A., van der Burg, M., Szuhai, K., Kops, G.J.P.L., Medema, R.H., 2011. Chromosome segregation errors as a cause of DNA damage and structural chromosome aberrations. Science 333 (6051), 1895–1898. https://doi.org/10.1126/science.1210214.

Kim, H.J., Kim, H.J., Kim, S.H., Kim, T.Y., 2003. Tetraacetyl phytosphingosine-induced caspase activation and apoptosis occur through G2 arrest in human keratinocyte HaCaT cells. J. Investig. Dermatol. 121 (5), 1135–1137. https://doi.org/10.1046/j.1523-1747.2003.12553.x.

Kolman, A., 2003. New achievements in human cell toxicology: the 20th annual workshop on in vitro toxicology. Altern. Lab. Anim. 31 (3), 241–243. https://doi.org/10.1177/026119290303100305.

Krewski, D., Andersen, M.E., Tyshenko, M.G., Krishnan, K., Hartung, T., Boekelheide, K., et al., 2020. Toxicity testing in the 21st century: progress in the past decade and future perspectives. Arch. Toxicol. 94 (1), 1–58. https://doi.org/10.1007/s00204-019-02613-4.

Lee, J.S., Min, D.S., Park, C., Park, C.S., Cho, N.J., 2001. Phytosphingosine and C2-phytoceramide induce cell death and inhibit carbachol-stimulated phospholipase D activation in Chinese hamster ovary cells expressing the *Caenorhabditis elegans* muscarinic acetylcholine receptor. FEBS Lett. 499 (1–2), 82–86. https://doi.org/10.1016/s0014-5793(01)02527-3.

Li, J., Wen, J., Sun, C., Zhou, Y., Xu, J., MacIsaac, H.J., Chang, X., Cui, Q., 2022. Phytosphingosine-induced cell apoptosis via a mitochondrially mediated pathway. Toxicology 482, 153370. https://doi.org/10.1016/j.tox.2022.153370.

Liang, Y., Feng, G., Wu, L., Zhong, S., Gao, X., Tong, Y., et al., 2019. Caffeic acid phenethyl ester suppressed growth and metastasis of nasopharyngeal carcinoma cells by inactivating the NF-κB pathway. Drug Des., Dev. Ther. 13, 1335–1345. https://doi.org/10.2147/DDDT.S199182.

Maceyka, M., Harikumar, K.B., Milstien, S., Spiegel, S., 2012. Sphingosine-1-phosphate signaling and its role in disease. Trends Cell Biol. 22 (1), 50–60. https://doi.org/10.1016/j.tcb.2011.09.003.

Mashima, R., Okuyama, T., Ohira, M., 2020. Biosynthesis of long-chain base in sphingolipids in animals, plants and fungi. Future Sci. OA. 6 (1). FSO 434. https://doi.org/10.2144/fsoa-2019-0094.

Nagahara, Y., Shinomiya, T., Kuroda, S., Kaneko, N., Nishio, R., Ikekita, M., 2005. Phytosphingosine induced mitochondria-involved apoptosis. Cancer Sci. 96 (2), 83–92. https://doi.org/10.1111/j.1349-7006.2005.00012.x.

Palus, J., Dziubałtowska, E., Stańczyk, M., Lewińska, D., Mankiewicz-Boczek, J., Izydorczyk, K., et al., 2007. Biomonitoring of cyanobacterial blooms in Polish water reservoir and the cytotoxicity and genotoxicity of selected cyanobacterial extracts. Int. J. Occup. Med. Environ. Health 20 (1), 48–65. https://doi.org/10.2478/v10001-007-0008-2.

Park, M.T., Choi, J.A., Kim, M.J., Um, H.D., Bae, S., Kang, C.M., et al., 2003a. Suppression of extracellular signal-related kinase and activation of p38 MAPK are two critical events leading to caspase-8- and mitochondria-mediated cell death in phytosphingosine-treated human cancer cells. J. Biol. Chem. 278 (50), 50624–50634. https://doi.org/10.1074/jbc.M309011200.

Park, M.T., Kang, J.A., Choi, J.A., Kang, C.M., Kim, T.H., Bae, S., 2003b. Phytosphingosine induces apoptotic cell death via caspase 8 activation and Bax translocation in human cancer cells. Clin. Cancer Res. 9 (2), 878–885. ⟨https://www.ncbi.nlm.nih.gov/pubmed/12576463⟩.

Poulsen, C., Mehalick, L.A., Fischer, C.L., Lanzel, E.A., Bates, A.M., Walters, K.S., et al., 2015. Differential cytotoxicity of long-chain bases for human oral gingival epithelial keratinocytes, oral fibroblasts, and dendritic cells. Toxicol. Lett. 237 (1), 21–29. https://doi.org/10.1016/j.toxlet.2015.05.012.

Rasheed, T., Bilal, M., Nabeel, F., Adeel, M., Iqbal, H., 2019. Environmentally-related contaminants of high concern: Potential sources and analytical modalities for detection, quantification, and treatment. Environ. Int. 122, 52–66. https://doi.org/10.1016/j.envint.2018.11.038.

Rashid, S.T., Harding, S.M., Law, C., Coackley, C., Bristow, R.G., 2011. Protein-protein interactions occur between p53 phosphoforms and ATM and 53BP1 at sites of exogenous DNA damage. Radiat. Res. 175 (5), 588–598. https://doi.org/10.1667/RR2084.1.

Rehberger, K., Kropf, C., Segner, H., 2018. In vitro or not in vitro: a short journey through a long history. Environ. Sci. Eur. 30 (1), 23. https://doi.org/10.1186/s12302-018-0151-3.

Sanchez-Baracaldo, P., Bianchini, G., Wilson, J.D., Knoll, A.H., 2022. Cyanobacteria and biogeochemical cycles through Earth's history. Trends Microbiol 30 (2), 143–157. https://doi.org/10.1016/j.tim.2021.05.008.

Singh, N.P., McCoy, M.T., Tice, R.R., Schneider, E.L., 1988. A simple technique for quantitation of low levels of DNA damage in individual cells. Exp. Cell Res. 175 (1), 184–191. https://doi.org/10.1016/0014-4827(88)90265-0.

Srinivas, U.S., Tan, B.W.Q., Vellayappan, B.A., Jeyasekharan, A.D., 2019. ROS and the DNA damage response in cancer. Redox Biol. 25, 101084 https://doi.org/10.1016/j.redox.2018.101084.

Sukharevich, V.I., Polyak, Y.M., 2021. Global occurrence of cyanobacteria: causes and effects. Inland Water Biol. 13 (4), 566–575. https://doi.org/10.1134/S1995082920060140.

Svircev, Z., Baltić, V., Gantar, M., Juković, M., Stojanović, D., Baltić, M., 2010. Molecular aspects of microcystin-induced hepatotoxicity and hepatocarcinogenesis. J. Environ. Sci. Health, Part C: Environ. Carcinog. Ecotoxicol. Rev. 28 (1), 39–59. https://doi.org/10.1080/10590500903585382.

Taha, T.A., Mullen, T.D., Obeid, L.M., 2006. A house divided: ceramide, sphingosine, and sphingosine-1-phosphate in programmed cell death. Biochim. Biophys. Acta 1758 (12), 2027–2036. https://doi.org/10.1016/j.bbamem.2006.10.018.

Umbuzeiro, G.A., Heringa, M., Zeiger, E., 2017. In vitro genotoxicity testing: significance and use in environmental monitoring. Adv. Biochem. Eng. /Biotechnol. 157, 59–80. https://doi.org/10.1007/10_2015_5018.

Velazquez, F.N., Hernandez-Corbacho, M., Trayssac, M., Stith, J.L., Bonica, J., Jean, B., et al., 2021. Bioactive sphingolipids: advancements and contributions from the laboratory of Dr. Lina M. Obeid. Cell. Signal. 79, 109875 https://doi.org/10.1016/j.cellsig.2020.109875.

Wang, C., Li, H., Ma, P., Sun, J., Li, L., Wei, J., et al., 2020. The third-generation retinoid adapalene triggered DNA damage to induce S-phase arrest in HaCat cells. Fundam. Clin. Pharmacol. 34 (3), 380–388. https://doi.org/10.1111/fcp.12527.

Wang, T., Chen, Z., Xie, P., Zhang, W., Du, M., Liu, Y., 2019. Isoliquiritigenin suppresses the proliferation and induced apoptosis via miR-32/LATS2/Wnt in nasopharyngeal carcinoma. Eur. J. Pharmacol. 856, 172352 https://doi.org/10.1016/j.ejphar.2019.04.033.

Xu, R., Jiang, Y., MacIsaac, H.J., Chen, L., Li, J., Xu, J., et al., 2019. Blooming cyanobacteria alter waterflea reproduction via exudates of estrogen analogues. Sci. Total Environ. 696, 133909 https://doi.org/10.1016/j.scitotenv.2019.133909.

Yagi, A., Hasegawa, Y., Xiao, H., Haneda, M., Kojima, E., Nishikimi, A., et al., 2003. GADD34 induces p53 phosphorylation and p21/WAF1 transcription. J. Cell. Biochem. 90 (6), 1242–1249. https://doi.org/10.1002/jcb.10711.

Zheng, G., Xu, R., Chang, X., Hilt, S., Wu, C., 2013. Cyanobacteria can allelopathically inhibit submerged macrophytes: effects of Microcystis aeruginosa extracts and exudates on *Potamogeton malaianus*. Aquat. Bot. 109, 1–7. https://doi.org/10.1016/j.aquabot.2013.02.004.

Zhou, Y., Xu, J., MacIsaac, H.J., McKay, R.M., Xu, R., Pei, Y., et al., 2023. Comparative metabolomic analysis of exudates of microcystin-producing and microcystin-free *Microcystis aeruginosa* strains. Front. Microbiol. 13, 1075621. https://doi.org/10.3389/fmicb.2022.1075621.

Zi, J., Pan, X., MacIsaac, H.J., Yang, J., Xu, R., Chen, S., et al., 2018. Cyanobacteria blooms induce embryonic heart failure in an endangered fish species. Aquat. Toxicol. 194, 78–85. https://doi.org/10.1016/j.aquatox.2017.11.007.

Zi, Y., Barker, J.,R., MacIsaac, H, J., Zhang, R., Gras, R., Chiang, Y.,C., et al., 2022. Identification of neurotoxic compounds in cyanobacteria exudate mixtures. Sci. Total Environ. 857 (Pt 2), 159257 https://doi.org/10.1016/j.scitotenv.2022.159257.

Zödl, B., Sargazi, M., Zeiner, M., Roberts, N.B., Steffan, I., Marktl, W., et al., 2004. Toxicological effects of iron on intestinal cells. Cell Biochem. Funct. 22 (3), 143–147. https://doi.org/10.1002/cbf.1065.

Further reading

Le Manach, S., Sotton, B., Huet, H., Duval, C., Paris, A., Marie, A., et al., 2018. Physiological effects caused by microcystin-producing and non-microcystin producing *Microcystis aeruginosa* on medaka fish: A proteomic and metabolomic study on liver. Environ. Pollut. 234, 523–537. https://doi.org/10.1016/j.envpol.2017.11.011.

Li, C., Tian, Q., Rahman, M.K.U., Wu, F., 2020. Effect of anti-fungal compound phytosphingosine in wheat root exudates on the rhizosphere soil microbial community of watermelon. Plant Soil 456 (1–2), 223–240. https://doi.org/10.1007/s11104-020-04702-1.

Pavicic, T., Wollenweber, U., Farwick, M., Korting, H.C., 2007. Anti-microbial and -inflammatory activity and efficacy of phytosphingosine: an in vitro and in vivo study addressing acne vulgaris. Int. J. Cosmet. Sci. 29 (3), 181–190. https://doi.org/10.1111/j.1467-2494.2007.00378.x.

Webster, M., Witkin, K.L., Cohen-Fix, O., 2009. Sizing up the nucleus: nuclear shape, size and nuclear-envelope assembly. J. Cell Sci. 122 (Pt10), 1477–1486. https://doi.org/10.1242/jcs.037333.